Journal of the European Ceramic Society **19** (1999) 399–405

PII: S0955-2219(98)00178-2
0955-2219/99/$—see front matter

Sintering of Cr_2O_3 in H_2/H_2O Gas Mixtures

T. Li,* R. J. Brook, and B. Derby

Department of Materials, University of Oxford, Oxford, OX1 3PH, UK

(Received 6 April 1998; accepted 20 July 1998)

Abstract

Sintering of Cr_2O_3 was performed at 1530°C under low pO_2 close to the Cr–Cr_2O_3 equilibrium generated by H_2/H_2O gas mixtures. Addition of 1 wt% ZrO_2 and 0·1 wt% MgO increases the density of Cr_2O_3 from 97% TD to nearly full density. Rapid densification and the higher density are attributed to the appearance of a transient CrO liquid phase as a result of the presence of ZrO_2 and MgO under the sintering conditions. A grain size reduction is also achieved owing to the presence of ZrO_2 particles and the possible formation of a $MgCr_2O_4$ spinel at grain boundaries. There is no connection between densification and loss of material due to evaporation.

Keywords: sintering, Cr_2O_3, microstructure – final, grain size, transition metal oxides.

1 Introduction

Sintering of Cr_2O_3 at atmospheric or near-atmospheric oxygen pressure yields a highly porous and partially sintered structure with little densification. Hagel *et al.*[1] used an argon atmosphere with $pO_2 \approx 10^{-2}$ Torr or 10^{-4} atm to study initial sintering but were unable to obtain a high density product. However, Ownby *et al.*[2] have demonstrated that, when oxygen pressures are near the Cr/Cr_2O_3 stability boundary, considerable densification takes place with specimens reaching almost theoretical density. These results have been confirmed by Halloran *et al.*[3], who studied the dependence of the initial sintering of chromia on oxygen partial pressure.

In an oxidizing atmosphere, Cr_2O_3 becomes unstable and vaporizes to form higher oxides of chromium, such as CrO_3. Promoting vapour phase transport, a high vapour pressure increases neck growth and coarsens particles but does not contribute to densification[2,4,5], while reducing the driving force for densification. Hench[6] concluded that both evaporation-condensation and volume-diffusion mechanisms were responsible for the sintering of Cr_2O_3 in air. Since the only non-volatile oxide species for chromium is Cr_2O_3, it has been proposed that, for densification by sintering to occur, virtually all of the chromium must be maintained in a 3+ oxidation state which is the case when oxygen pressures are near the Cr/Cr_2O_3 stability boundary.[2] Roy *et al.*,[7] in their study of isothermal sintering kinetics of Cr_2O_3 in the presence of varying amounts of MgO at temperatures up to 1500°C in C powder, found that sintering was predominantly a grain boundary diffusion process with parallel vapour transport to varying extents, with an activation energy for densification between 140 and 158 kJ mol^{-1}.[7,8]

Under low oxygen partial pressures, doping Cr_2O_3 with 0.1 wt% MgO leads to a further increase in density to 99% theoretical density (TD) or 96% TD when sintered in CO/CO_2 gas mixtures or carbon powder, respectively. This effect is attributed to the nucleation of $MgCr_2O_4$ second-phase particles along the grain boundaries, inhibiting abnormal grain growth. However, MgO doping is effective only if the oxygen partial pressure of the sintering atmosphere is sufficiently reduced to maintain the Cr_2O_3 phase and if the undoped powder itself is sinterable to high density. Additions of La_2O_3[8] and TiO_2[9] have also been found to promote sintering of Cr_2O_3. The sintering mechanisms of Cr_2O_3 have been the subject of many studies. It is proposed that densification of Cr_2O_3 is controlled by oxygen vacancy diffusion.[10] However, there has been no single conclusive interpretation of the atmosphere dependent densification behaviour of Cr_2O_3.

In order to control the sintering atmosphere, two approaches are generally used: (1) immersing the sample in a carbon powder bed[7,8,11] or mixing carbon powder with the sample powder before shaping[12] and (2) sintering in a controlled CO/CO_2 gas mixture.[2,3,13] Sintering in a carbon powder bed is

*To whom corespondence should be addressed at: Materials Research Center, Lehigh University, 5 E. Packer Avenue, Bethlehem, PA 18015 USA.

commonly used for its simplicity and convenience in terms of equipment. The problems associated include: (a) the existence of a reaction layer between carbon and Cr_2O_3,[11] (b) too low a pO_2 (10^{-16}–10^{-18} atm) which can result in limited densification (up to 96% TD); and (c) possible contamination from the carbon source powder. On the other hand, for the CO/CO_2 buffer system, the pO_2 can be readily adjusted. However, deposition of carbon due to the high CO/CO_2 ratio necessary to generate a low pO_2 still casts doubt on results because of possible carbon contamination of samples.

To avoid contamination associated with using a CO/CO_2 gas mixture or carbon powder, the present study involves sintering Cr_2O_3 in low pO_2 atmospheres generated by using H_2O/H_2 gas mixtures; the effects of MgO and ZrO_2 additions on densification and the mechanisms involved have also been investigated.

2 Experimental Procedure

The starting materials were 99·9 wt% pure Cr_2O_3 powder (Aldrich Co.) with an average particle size $\sim 0{\cdot}4$ μm, 99·9% pure MgO powder (Aldrich Co.) with an average particle size of $\sim 0{\cdot}2$ μm was used as an additive. These powders were wet ball-milled for 4 h in ethyl alcohol (> 99·7 vol%) with 3 wt% MgO stabilized tetragonal-ZrO_2 balls (∅10 mm), so as to homogenize the powder mixture. The mass ratio of the milling media to the material was 10 to 1. ZrO_2 balls became worn in the milling process, acting as a source of ZrO_2 addition. The amount of ZrO_2 added was controlled by adjusting the ball-milling intensity. After ball-milling, the slurry was dried under an infrared lamp for 12 h. Next, the powder mixture was crushed with a mortar and pestle before passing through a 65 μm sieve. Green compacts of Cr_2O_3 and $Cr_2O_3 + 0{\cdot}1$ wt% MgO + 1 wt% ZrO_2 in the form of cylindrical pellets ($\approx$∅11·0×3·0 mm) with densities between 62 and 65% TD were formed by pressing uniaxially in hard steel dies at $\approx$300 MPa.

Cr_2O_3 or $Cr_2O_3 + 0.1$ wt% MgO + 1 wt% ZrO_2 green compacts was sintered under controlled atmosphere conditions. At temperatures below 1400°C, flowing Ar was used. When the temperature was increased further, a controlled atmosphere generated by adjusting the ratio of H_2/H_2O vapor was introduced. The flow rates for both Ar and H_2/H_2O were 20–40 ml min^{-1}. Cooling was conducted in flowing Ar at a rate of 8°C min^{-1}. Oxygen partial pressure inside the furnace was continuously monitored *in situ* with an oxygen sensor based on 5 wt% CaO stabilized ZrO_2. Sintered densities were measured using the immersion method (water). The dimensions of the green bodies were obtained by direct measurment. A computerized pushrod dilatometer (Dilatronic© IIRDP) was employed to measure the dimensional changes of the powder compacts during oxidation with an accuracy of 0·5%. Element content, phase and microstructure were characterized using X-ray diffraction (XRD) (Philips 1310 with copper Kα radiation at 40 kV, 20 mA), scanning electron microscopy (SEM) (PHILIPS 501) coupled with microanalysis using energy dispersive spectroscopy (EDS) and by electron probe microanalysis (EPMA) (CAMECA SEMPROBE Model SU30 in conjunction with a wavelength dispersive spectrometer).

3 Results and Discussion

3.1 Oxygen partial pressure dependence

To avoid possible problems of carbon deposition involved in the use of a CO/CO_2 gas mixture, a H_2/H_2O buffer was used in this investigation to establish a series of controlled oxygen partial pressures. The effects of oxygen partial pressure on final density and weight loss for both Cr_2O_3 and $Cr_2O_3 + 1$ wt% $ZrO_2 + 0{\cdot}1$ wt% MgO samples sintered at 1530°C for 1 h are displayed in Figs 1 and 2, respectively. Maximum densification is achieved for both samples when the oxygen partial pressure is around the Cr–Cr_2O_3 equilibrium pressure. The final densities of $Cr_2O_3 + 1$ wt% ZrO_2 + 0·1 wt% MgO samples are always a few percent higher than those of Cr_2O_3 samples. This supports the results of Ownby *et al.*[2] and Roy *et al.*,[7] who conducted their sintering experiments in CO/CO_2 and a carbon powder bed, respectively.

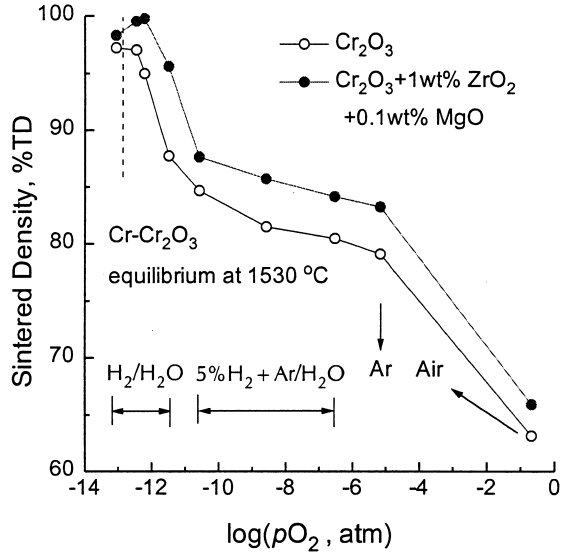

Fig. 1. Effect of pO2 on final density. Oxygen partial pressures are established in various gas mixtures as indicated in the figure. Sintering condition: 1530°C for 1 h. Green density: 62–66%TD.

There are a number of volatile species that may exist over Cr_2O_3 at high temperatures from Cr(g), CrO(g) at low oxygen partial pressures to CrO_3(g) at high oxygen partial pressures. Under atmospheric or near atmospheric oxygen partial pressures, weight loss occurs because of the volatile CrO_3. At high temperatures and low oxygen partial pressures close to the Cr–Cr_2O_3 equilibrium, Cr and CrO may be formed. The subsequent evaporation of these species may account for most of the observed weight loss. Experimentally, many factors affect the percentage weight loss of Cr_2O_3, such as processing temperature, soaking time, oxygen partial pressure, total gas pressure, flow rate and the ratio of total surface to weight. Under identical experimental conditions, the dependence of weight loss on the oxygen partial pressure is shown in Fig. 2. The general trend is for the weight loss to increase with a decrease in oxygen partial pressure. Cr_2O_3 + 1 wt% ZrO_2 + 0·1 wt% MgO samples show larger weight loss than undoped samples at low oxygen partial pressures.

3.2 Dilatometry

Dilatometric studies of the densification behaviour of Cr_2O_3 + 1 wt% ZrO_2 + 0·1 wt% MgO and Cr_2O_3 are displayed in Fig. 3. During the experiment, Ar was used at temperatures below 1350°C followed by the introduction of H_2/H_2O at temperatures up to 1530°C for 1 h. The sudden decrease in volume of the Cr_2O_3 + 1 wt% ZrO_2 + 0·1 wt% MgO sample at the beginning of the experiment is due to evaporation of volatile species such as water, H_2, CO, CO_2, C_xH_y and alcohols from wet ball-milling in ethyl alcohol. The Cr_2O_3 sample underwent only a little shrinkage due to the evaporation of absorbed water and other volatile impurities, because no ball milling processing stage was involved.

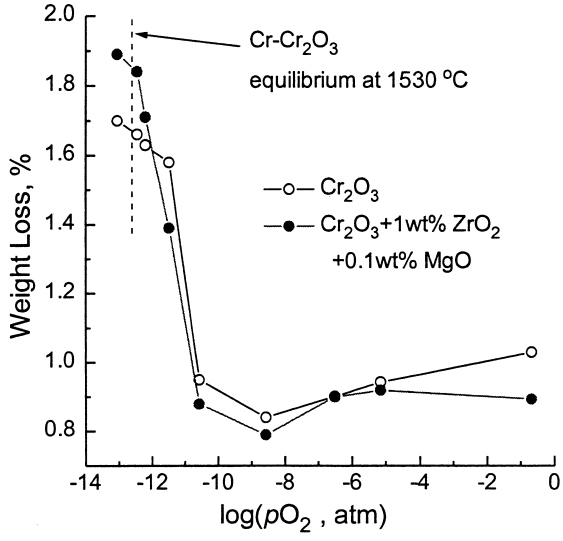

Fig. 2. Effect of pO_2 on weight loss after sintering at 1530°C for 1 h. Green density: 62–66% TD.

With an increase in temperature to over 1000°C, both samples started to shrink. Sintering of the Cr_2O_3 sample is always slower than that of the Cr_2O_3 + 1 wt% ZrO_2 + 0·1 wt% MgO sample. Under an oxygen partial pressure of $3{\cdot}4\times10^{-13}$ atm, the samples achieved final densities of 96 and 99% TD, respectively. When cooling in Ar, the Cr_2O_3 + 1 wt% ZrO_2 + 0·1 wt% MgO sample underwent a 0·5% linear expansion.

3.3 Microstructure

Figure 4 shows backscattered SEM micrographs of thermally etched samples of Cr_2O_3 + 1 wt% ZrO_2 + 0·1 wt% MgO and Cr_2O_3. It can be seen that the Cr_2O_3 sample exhibits a 'clean' microstructure, whereas a second phase exists in the Cr_2O_3 samples doped with 1 wt% ZrO_2 and 0·1 wt% MgO as indicated by the presence of a white phase inside grains and along grain boundaries. This contrast in backscattered imaging indicates a greater mean atomic number for the second phase than for the Cr_2O_3 grains. EDS results have revealed that this white phase always contains Zr and in some instances Mg, apart from Cr. EPMA analysis has also shown strips of a Mg-containing grey phase are present mainly along grain boundaries. The amount of the grey phase (larger than 0·1 wt%) suggests that it is the spinel $MgCr_2O_4$,[2,7] due to the reaction of MgO with Cr_2O_3 under the sintering conditions.[4,14]

A second phase peak was detected by XRD as shown in Fig. 5, which has not been identified. The distribution of the intergranular white phase observed on a free surface of the doped sample after 8 h at the sintering temperature (Fig. 6), suggests that a transient liquid phase might be formed during the densification stage.

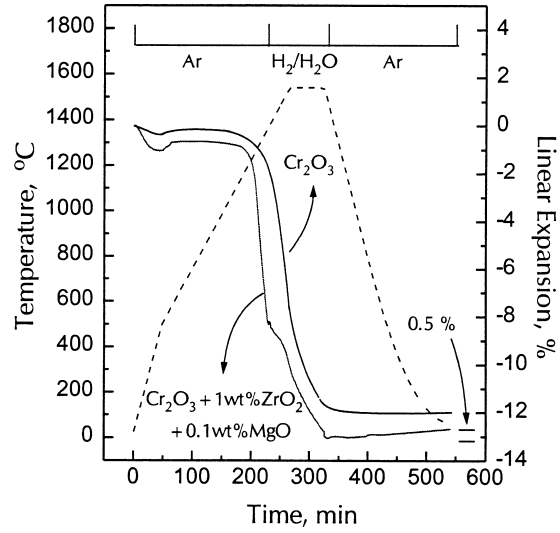

Fig. 3. Dilatometer measurement of sintering behaviour of Cr_2O_3 and Cr_2O_3 + 1 wt% ZrO_2 + 0·1 wt% MgO powder compacts. Green density: 65 % TD. The broken line represents the temperature profile during the experiment.

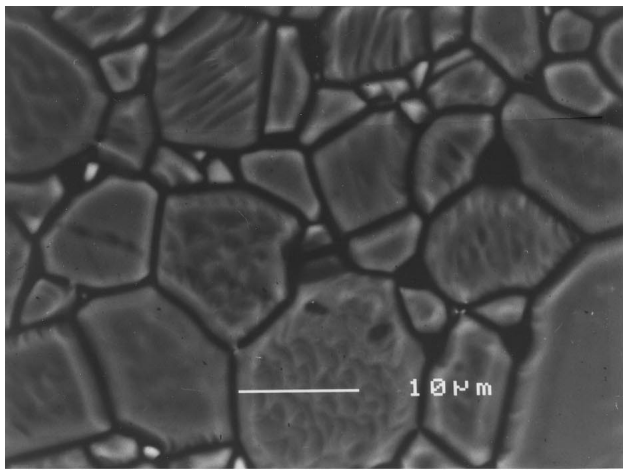

A: Cr_2O_3

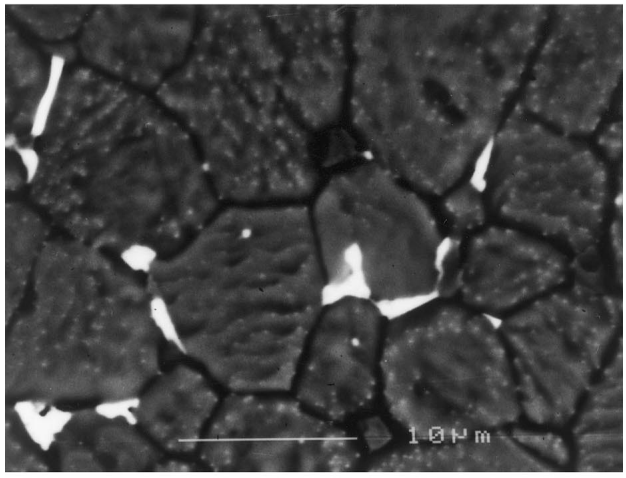

B: Cr_2O_3+1wt%ZrO_2+0.1wt%MgO

Fig. 4. Backscattered SEM micrographs of the microstiructure of thermally etched samples. The presence of white areas along grain boundaries in micrograph A is due to the edge effect.

For both types of samples with densities between 95 and 99% TD, the change of mean grain size with sintering time is displayed in Fig. 7. The grain sizes of Cr_2O_3 samples are found to be consistently bigger than those of Cr_2O_3 + 1 wt% ZrO_2 + 0·1 wt% MgO samples. Grain growth in the Cr_2O_3 samples was approximately proportional to the square root of time, as is typical for grain growth in pure, single phase solids.

3.4 Sintering mechanisms

Sintering governed by lattice diffusion is dependent upon point defects. Densification can be optimised by close control of impurities and the ambient partial pressure of oxygen. Based on the defect structure model where Cr interstitials and O vacancies are the important defects near the Cr/Cr_2O_3 boundary, Kofstad has proposed that the

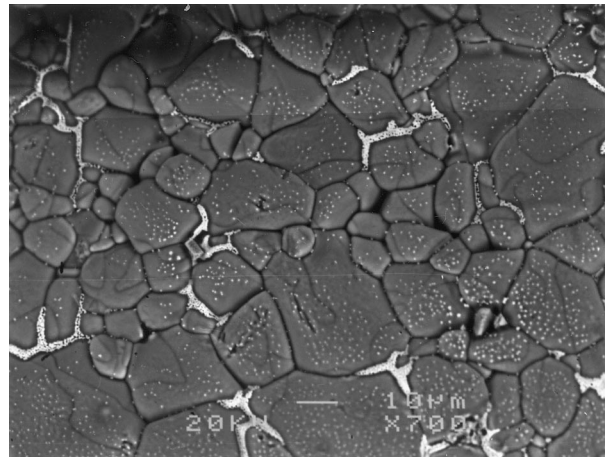

Fig. 6. SEM micrograph of a free surface of a Cr_2O_3 + 1 wt% ZrO_2 + 0·1 wt% MgO sample showing the distribution of the white phase between grains.

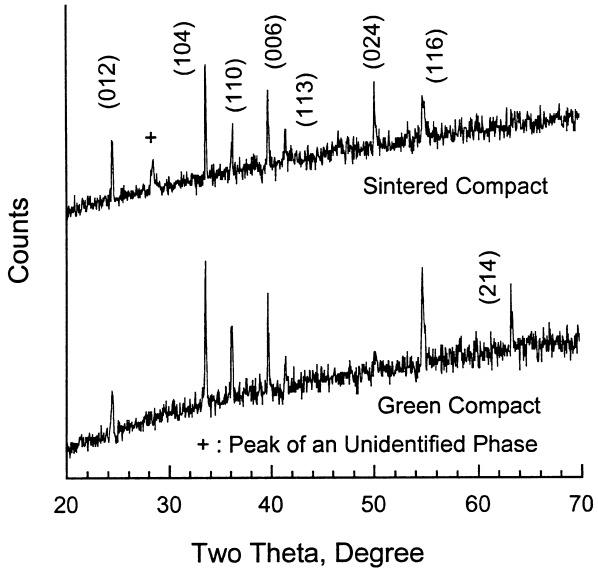

Fig. 5. XRD patterns of a Cr_2O_3 + 1 wt% ZrO_2 + 0·1 wt% MgO sample before and after sintering. The indices are those of Cr_2O_3.

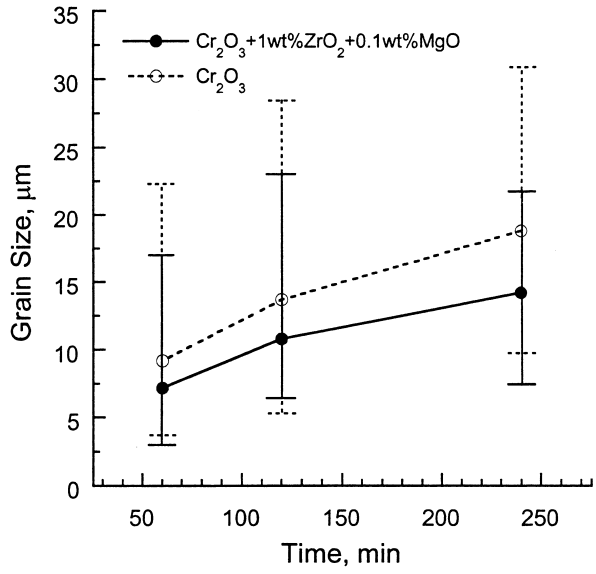

Fig. 7. Mean grain size of Cr_2O_3 + 1 wt% ZrO_2 + 0·1 wt% MgO and Cr_2O_3 versus sintering time. Error bars indicate the maximum and minimum grain sizes measured.

sintering of Cr_2O_3 is governed by oxygen vacancy diffusion.[10]

As illustrated in Fig. 3, Cr_2O_3 sinters faster in the presence of 1 wt% ZrO_2 + 0·1 wt% MgO, compared with undoped Cr_2O_3. From the phase diagram of the Cr_2O_3–ZrO_2 system as shown in Fig. 8,[15] there is very little solubility between Cr_2O_3 and ZrO_2 in the solid state. However, the two oxides are miscible in the liquid state, and the eutectic point (1850 ± 10°C) is much lower than the melting points of the two pure oxides. If a regular solution model is assumed for the liquid phase in the Cr_2O_3–ZrO_2 system (see the Appendix), the analysis indicates that there is a strong tendency for Cr_2O_3 and ZrO_2 to form a liquid Cr–Zr–O phase.

Toker's work on the Cr–Cr_2O_3 phase diagram[16] shows the stability range for liquid CrO extending to lower temperatures in the presence of dissolved impurity phases. Mg and Fe impurities are also known to extend the stability range of oxides containing Cr^{2+} ions.

Using the Gibbs free energy data for CrO, Cr_3O_4 and Cr_2O_3 formation given by Toker,[16] the stability ranges in terms of temperature and oxygen partial pressure for different phases at unit activity have been calculated and are shown schematically in Fig. 9. For pure materials, the liquid phase CrO is stable over a narrow region at high temperatures and low oxygen partial pressures. When liquid CrO is not pure but mixed with impurities, e.g. ZrO_2, the formation of a liquid Cr–Zr–O phase is favoured. Figure 10 displays a temperature–oxygen partial pressure relationship when the activity of CrO is 0·8 and all the other phases are at unit activity. The domain where a liquid CrO phase is stable is extended to temperatures as low as 1450°C and to a great range of oxygen partial pressures. In this investigation, the optimum sintering condition (at 1530°C under an oxygen partial pressure of

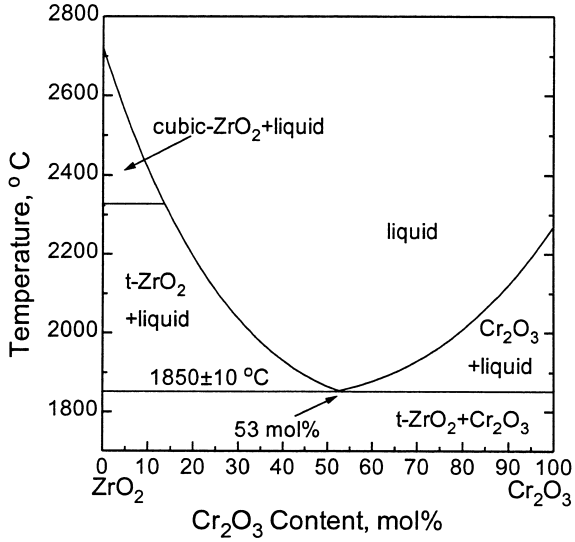

Fig. 8. Cr_2O_3–ZrO_2 phase diagram.[15]

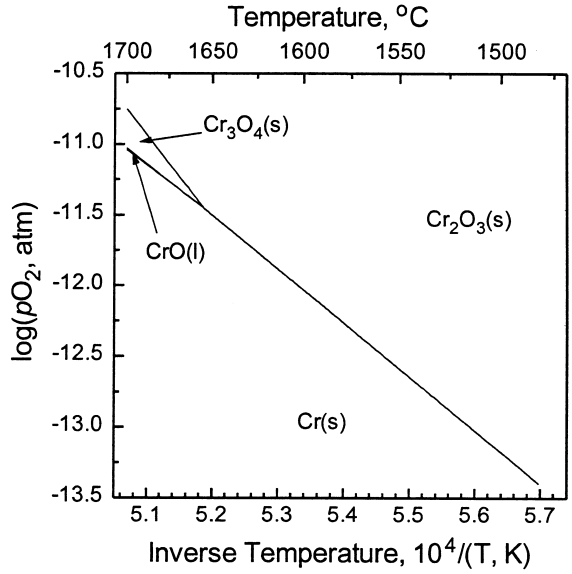

Fig. 9. Diagram showing the regimes of temperature and $pO2$ in which various chromium oxides are stable. All components are in unit activity.

$10^{-12.5}$ atm) lies in this domain, giving further evidence for the possible existence of a transient liquid CrO phase during densifilcation of Cr_2O_3 + 1 wt% ZrO_2 + 0·1 wt% MgO.

Factors affecting solid solution formation include relative ionic radius, valence, chemical affinity and structural similarity. To form wide ranges of solid solubility, both components must have comparable properties, i.e., similar ionic radii, isovalence, similar structures and a low chemical affinity (i.e., they do not form compounds).[17] Cr_2O_3 and ZrO_2 do not react to form a compound. Zr^{4+} has an ionic radius of 0·081 nm.[18] For chromium oxides, the ionic radius of Cr^{2+} is 0·085 nm for its high spin configuration and 0·076 nm for its low spin configuration, whereas Cr^{3+} has an ionic

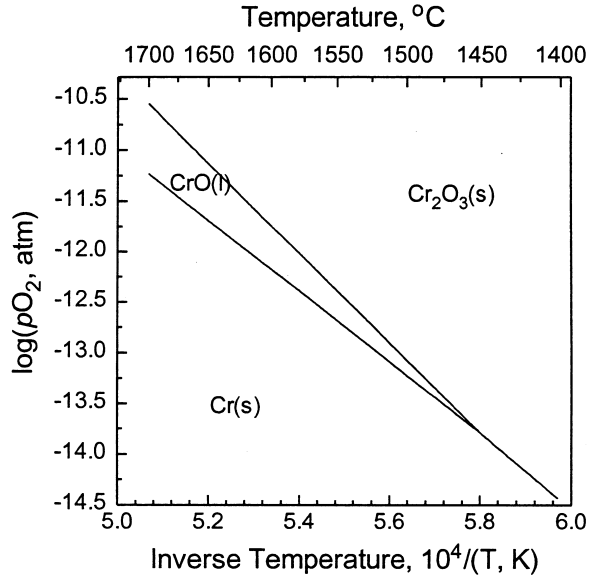

Fig. 10. Diagram showing the stability ranges of chromium and its oxides assuming unit activity for all except CrO, which is given as 0·8.

radius of 0·066 mn.[18] A possible sequence of events is accordingly as follows. From size similarity, more Zr^{4+} ions should dissolve in CrO than in Cr_2O_3. Since the chromium oxide adjacent to grain boundaries is more susceptible to the atmosphere, CrO is formed initially in these areas. On cooling under Ar, Cr^{2+} ions become oxidized to Cr^{3+}. Due to a decrease in solubility of Zr^{4+} with this change, Zr^{4+} precipitates during cooling, the white Zr-containing phase being mainly distributed in areas near the grain boundaries (Fig. 4).

Experimental results show that weight loss increases when densification is at a maximum (cf. Figures 1 and 2) and the weight loss of $Cr_2O_3 + 1$ wt% $ZrO_2 + 0{\cdot}1$ wt% MgO is higher than that of Cr_2O_3 (Fig. 2). This phenomenon can be explained by the evaporation of Cr(g) and CrO(g), especially CrO(g) in the case of $Cr_2O_3 + 1$ wt% $ZrO_2 + 0{\cdot}1$ wt% MgO due to the presence of a transient liquid CrO. Therefore, there is no inverse connection between weight loss and the sintering rate.

4 Conclusions

1. Cr_2O_3 has been sintered to high density (up to 97% TD) at 1530°C in atmospheres with oxygen partial pressures close to the Cr–Cr_2O_3 equilibrium, controlled by H_2/H_2O gas mixtures.
2. The grain sizes of $Cr_2O_3 + 1$ wt% $ZrO_2 + 0{\cdot}1$ wt% MgO samples are consistently smaller than those of Cr_2O_3 samples. The presence of a Zr-containing phase and possible formation of a $MgCr_2O_4$ spinel at grain boundaries are associated with the reduction in grain growth.
3. Under the same sintering conditions, addition of 1 wt% ZrO_2 and 0·1 wt% MgO increases the density of Cr_2O_3 to nearly full density in a shorter period of time. The rapid densification and higher final density are attributed to the appearance of a transient CrO liquid phase whose activity was lowered by the presence of ZrO_2 and MgO under low oxygen partial pressures and high temperatures. Loss of material due to evaporation does not prevent densification.

Acknowledgements

The authors wish to thank P. Xiao for his help on thermodynamic calculations.

References

1. Hagel, W. C., Jorgensen, P. J. and Tomalin, D. S., Initial sintering of α-Cr_2O_3. *J. Am. Ceram. Soc.*, 1966, **49**, 23–26.
2. Ownby, P. D. and Jungquist, G. E., Final sintering of Cr_2O_3. *J. Am. Ceram. Soc.*, 1972, **55**, 433–436.
3. Halloran, J. W. and Anderson, H. U., Influence of O_2 partial pressure on initial sintering of α-Cr_2O_3. *J. Am. Ceram. Soc.*, 1974, **57**, 150.
4. Anderson, H. U., Influence of oxygen activity on the sintering of $MgCr_2O_4$. *J. Am. Ceram. Soc.*, 1974, **55**, 34–37.
5. Ownby, P. D., Oxidation state control of volatile species in sintering. In *Matetials Science Research*, Vol. 6, ed. G. C. Kuczynski. Plenum Press, New York, 1973, pp. 431–437.
6. Hench, L. L. Sintering and reactions of magnesia and chromia. Ph.D. thesis, Ohio State University, Columbus, OH, 1964.
7. Roy, S. N., Saha, S. R. and Guha, S. K., Sintering kinetics of pure and doped chromium oxide. *J. Mater. Sci.*, 1986, **21**, 3673–3676.
8. Roy, S. N., Guha, S. K. and Maiti, H. S., Studies on the influence of lanthanum oxide on the sinterability of chromium(III) oxide. *J. Mater. Sci.*, 1990, **25**, 3508–3512.
9. Callister, W. D., Johnson, M. L., Cutler, I. B. and Ure Jr, R. W., Sintering chromium oxide with the aid of TiO_2. *J. Am. Ceram. Soc.*, 1979, **62**, 208–211.
10. Kofstad, P., *High Temperature Corrosion*, Elsevier Applied Science, New York, 1988.
11. Yamaguchi, A., Sintering of Cr_2O_3 in carbon powder. *Joumal of the Ceramic Society of Japan*, 1980, **88**, 184–190.
12. Stone, H. E. N., Sintering in chromic oxide. *Metallurgia*, 1968, April, 152–154.
13. Neve, J. M. and Coble, R. L., Initial sintering of Cr_2O_3. *J. Am. Ceram. Soc.*, 1974, **57**, 274–275.
14. Ulmer, G. C. and White, W. B., Existence of chromium ion in the spinel solid solution series $FeCr_2O_4$–$MgCr_2O_4$. *J. Am. Ceram. Soc.*, 1966, **49**(1), 50–51.
15. Lopato, L. M., Shevchenko, A. V. and Maister, I. M., Reaction of ZrO_2 with Cr_2O_3. *Inorganic Materials*, 1977, **13**(10), 1467–1469.
16. Toker, N. Y., Equilibrium phase relation and thermodynamics for the systems chromium–oxygen and iron–chromium–oxygen in the temperature range from 1500–1825°C. Ph.D thesis, PennState University, State College, PA, 1977.
17. Kingery, W. D., Bowen, H. K. and Uhlman, D. R., *Introduction to Ceramics*, 2nd ed. Wiley, New York, 1976.
18. Shannon, R. D. and Prewitt, C. T., Effective ionic radii in oxides and fluorides. *Acts. Cryst.*, 1969, **B25**, 925–946.

Appendix

Application of a regular solution model to the liquid phase in the Cr_2O_3-ZrO_2 system

Cr_2O_3 is taken as component 1, and ZrO_2 as component 2. For a liquid phase rich in Cr_2O_3, the formula relating the interaction parameter, α_{12}, to the activity coefficient, γ_1^l, of Cr_2O_3 in a liquid state is given by:

$$RT \ln \gamma_1^l = \alpha_{12}(1 - \chi_1^l)^2 \qquad \text{(A1)}$$

where χ_1^l the fraction of component 1 (Cr_2O_3) in the liquid.

The chemical potential of Cr_2O_3 in a liquid phase can be expressed as:

$$\mu_1^l = \mu_1^{0l} + RT \ln a_1^l = \mu_1^{0l} + RT \ln \gamma_1^l + RT \ln \chi_1^l \qquad \text{(A2)}$$

where μ_1^{0l} is the chemical potential of the pure liquid component 1 and a_1^l is the activity of component 1 in the liquid.

At the melting temperature (T_{1m}) of Cr_2O_3, the equilibrium condition requires that

$$\mu_1^{0s}(T_{1m}) = \mu_1^{0l}(T_{1m}) \tag{A3}$$

At the eutectic point where $T = 1850°C$,

$$\mu_1^{0s}(T) = \mu_1^l(T) = \mu_1^l(T) = \mu_1^{0l} + RT\ln\gamma_1^l + RT\ln\chi_1^l \tag{A4}$$

The above equation can also be rewritten as:

$$\frac{\mu_1^{0s}(T) - \mu_1^{0l}(T)}{T} = R\ln\gamma_1^l + R\ln\chi_1^l \tag{A5}$$

According to the Gibbs–Helmholtz equation:

$$\frac{\mu_1^{0s} - \mu_1^{0l}}{T} - \frac{\mu_1^{0s}(T_{1m}) - \mu_1^{0l}(T_{1m})}{T_{1m}} = \int_{T_m}^{T} \frac{\Delta H_{1m}}{T^2}\,\mathrm{d}T = -\Delta H_{1m}^l\left[\frac{1}{T_{1m}} - \frac{1}{T}\right] \tag{A6}$$

Combining eqns (1), (3), (5) and (6), the interaction parameter α_{12} can be calculated by the following equation:

$$-\Delta H_{1m}^l\left[\frac{1}{T_{1m}} - \frac{1}{T}\right] = \frac{\alpha_{12}}{T}(1-\chi_1^l)^2 + R\ln\chi_1^l \tag{A7}$$

Likewise, following the same procedure, the interaction parameter for a liquid solute rich in ZrO_2, α_{21}, can also be derived:

$$-\Delta H_{2m}^l\left[\frac{1}{T_{2m}} - \frac{1}{T}\right] = \frac{\alpha_{21}}{T}(1-\chi_2^l)^2 + R\ln\chi_2^l \tag{A8}$$

The data used to calculated the interaction parameter are listed in Table A1 along with the calculated α results.

From Table A1, it can be seen that the two interaction parameters, α_{12} and α_{21}, are very negative and comparable with each other, indicating that there is a strong tendency for Cr_2O_3 and ZrO_2 to form a liquid Cr–Zr–O phase.

Table A1. Interaction parameters and the data used to calculate them

Items	Cr_2O_3	ZrO_2
Melting point (T_m), (°C)	2266	2700
Eutectic temperature (T), (°C)	1850	1850
Concentration at eutectic (χ^l), (mol%)	53	47
ΔH_m, (kJ mol^{-1})	−1140	−1100
Interaction Parameter (α), (kJ mol^{-1})	−795	−1072